Supplementary Material

Geothermal exploration in the Burwash Landing region, Canada, using three-dimensional inversion of passive electromagnetic data

Tschirhart, V.[1]*, Colpron, M.[2], Craven, J.[1], Hormozzade Ghalati, F.[3], Enkin, R.J.[4] and Grasby, S. E.[5]

[1] Geological Survey of Canada, Ottawa, ON, Canada.

[2] Yukon Geological Survey, Whitehorse, YT, Canada.

[3] Department of Earth Science, Carleton University, Ottawa, ON, K1S 5B6, Canada.

[4] Geological Survey of Canada, Sidney, BC, Canada.

[5] Geological Survey of Canada, Sidney, BC, Canada.

*Correspondence: Victoria.tschirhart@nrcan-rncan.gc.ca

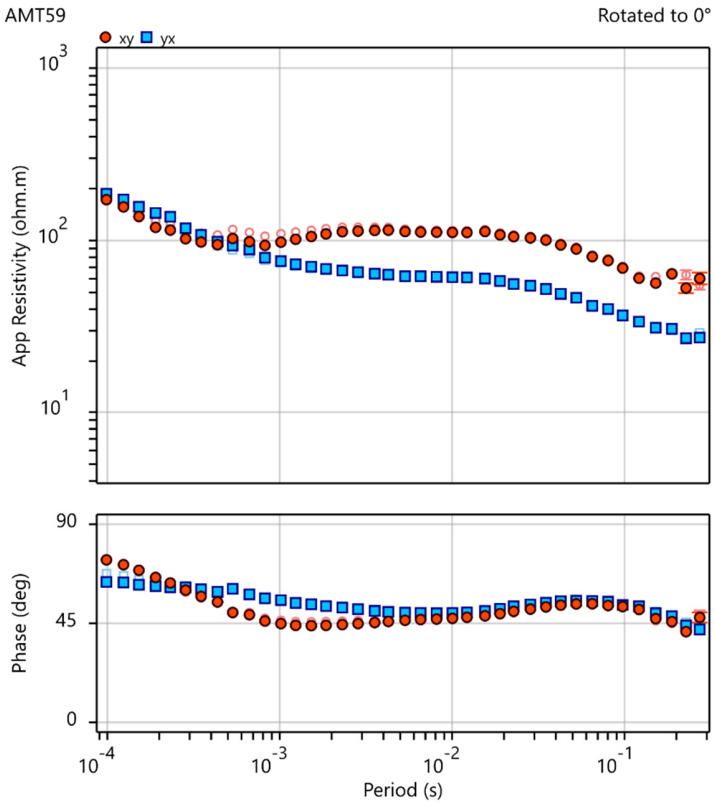
This supplementary document contains additional details on the electrode acquisition and 3D inversion parameter tests for the passive electromagnetic (EM) datasets used in the study.

1. Porous pots versus metal plates as electrodes

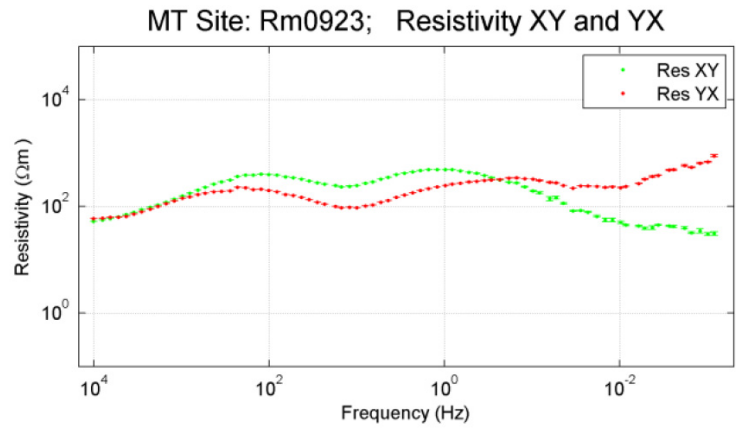
Initial acquisition of broadband magnetotelluric (BBMT) and audiomagnetotelluric (AMT) data followed standard field procedures, which requires the use of porous pots as electrodes (Chaves and Jones, 2012). Following discussions with the contractor, Quantec Geoscience, who advocated for the use of their pre-corroded proprietary steel plates as electrodes, we attempted data collection at two sites; however the overnight BBMT site was disturbed resulting in only data at one AMT site (AMT59) being collected using porous pots and plates for 90 minutes (Figure S1a). Additional documentation provided by the contractor showing BBMT electrode comparison tests for three 24 hour recording periods

showed no notable difference in data quality between porous pots and plates for referenced sites (Figure S1b, S1c), with there generally being only minor differences after 100 s in unreferenced sites (Quantec Geoscience, 2021). Following the AMT test and previous BBMT tests (Quantec Geoscience, 2021), the remaining AMT and BBMT stations were acquired using metal plates. In general, plates were much more cost effective in comparison to pots and have potential for greater longevity allowing for use over multiple field campaigns.

(a)



(b)



(c)

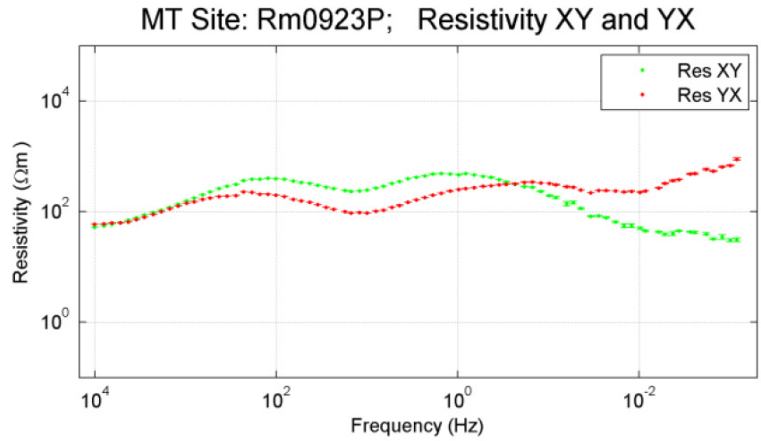


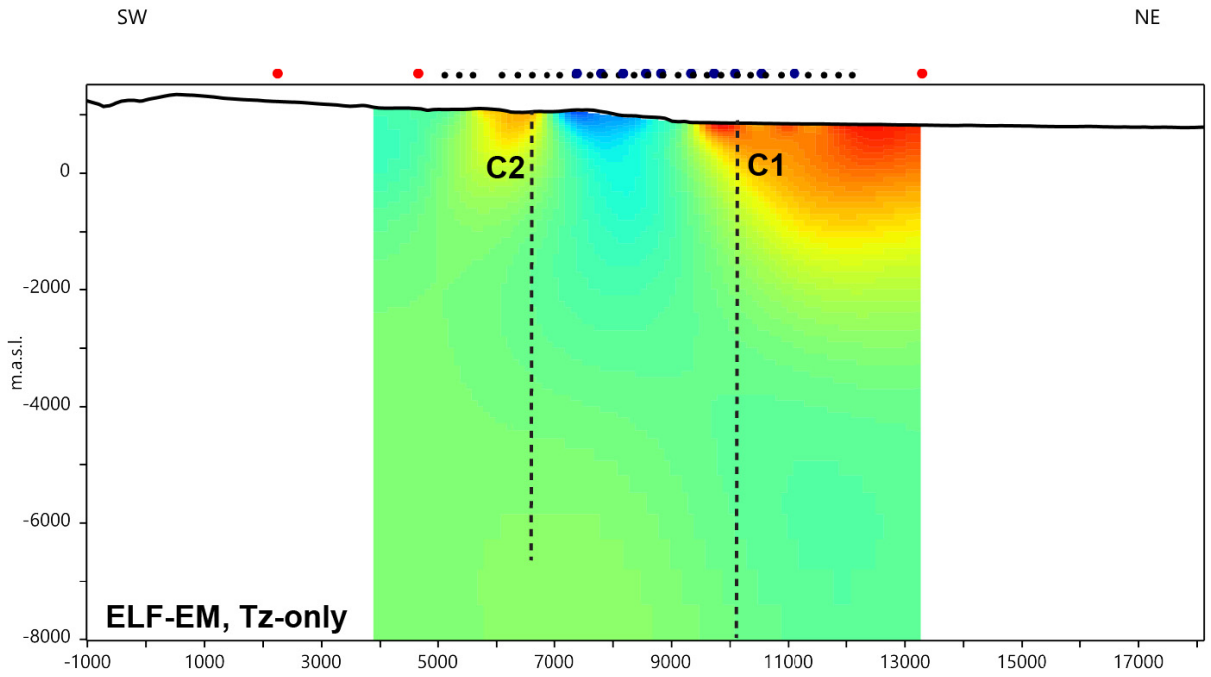
Figure S1: a) Apparent resistivity and phase curves for metal plates (red filled circles (xy) and blue filled squares (yx)) and porous pot electrodes (red outlined circles (xy) and blue outlined squares (yx)). b) Apparent resistivity for plates for 24 hour referenced site reprinted with permission from Quantec Geoscience (2021). © 2021, Quantec Geoscience. c) Apparent resistivity for pots for 24 hour referenced site reprinted with permission from Quantec Geoscience (2021). © 2021, Quantec Geoscience.

2. Inversion of Passive Electromagnetic Datasets

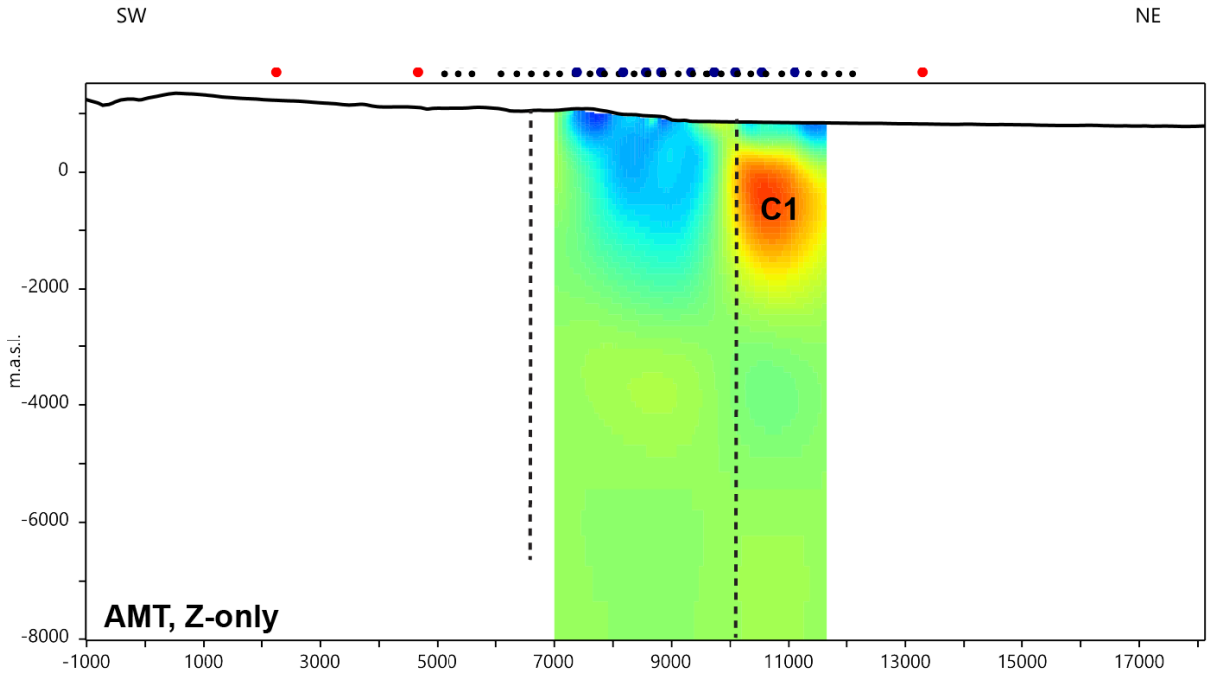
During the initial inversion testing in RLM-3D each geophysical dataset ((extremely low frequency electromagnetic (ELF-EM), AMT and MT) was individually inverted (Figure S2). The presence of certain features (e.g. C1, C2, C3 in Figure S2) across multiple datasets supports their likely requirement by the data. Additional inversions using different starting models, different error floors, various alpha smoothing parameters, topographic data, distortion matrix and exclusion of vertical magnetic transfer function (Tz) data (Figure S2d) were also tested (Table S1 and Figure S2). Forward tests were also performed on different half-space model (100 Ωm, 200 Ωm, 500 Ωm, and 1000 Ωm) to test the effect of topography on different models (results of 200 Ωm half-space tests are shown in Figure S3). These tests indicate that the preferred model (Figure 6d) inversion parameters are relatively optimal and the main conductivity features are robust. One MT and one AMT station had to be discarded from the inversion, five MT tippers were not included due to large error values, and two MT sites did not have tipper data collected. This resulted in 321 ELF stations, 51 MT stations and 33 AMT stations constituting the final inversion. Overall, the RMS misfit of the model is generally quite small, with larger errors present at the edges of the survey (e.g. MT100, MT105) and along the Denali fault (e.g. MT12). Additional examples of some fits for apparent resistivity, phase and tipper are shown in Figure S4.

	Parameter	Values
RLM3D	Mesh Cell Size (Horizontal)	**100 m**, 200 m, 300 m
	Starting Half space Value	100 Ωm, 2**00 Ωm**, 500 Ωm
	Alpha (x, y, z) parameters	1,1,1; 3,1,1; 1,3,1; **1,2,1**
	Vertical magnetic transfer functions	**Yes,** No
	Topography included	**Yes**, No
	Invert for distortion matrix	**Yes**, No
	Data Error Floor	**5%,** 10%

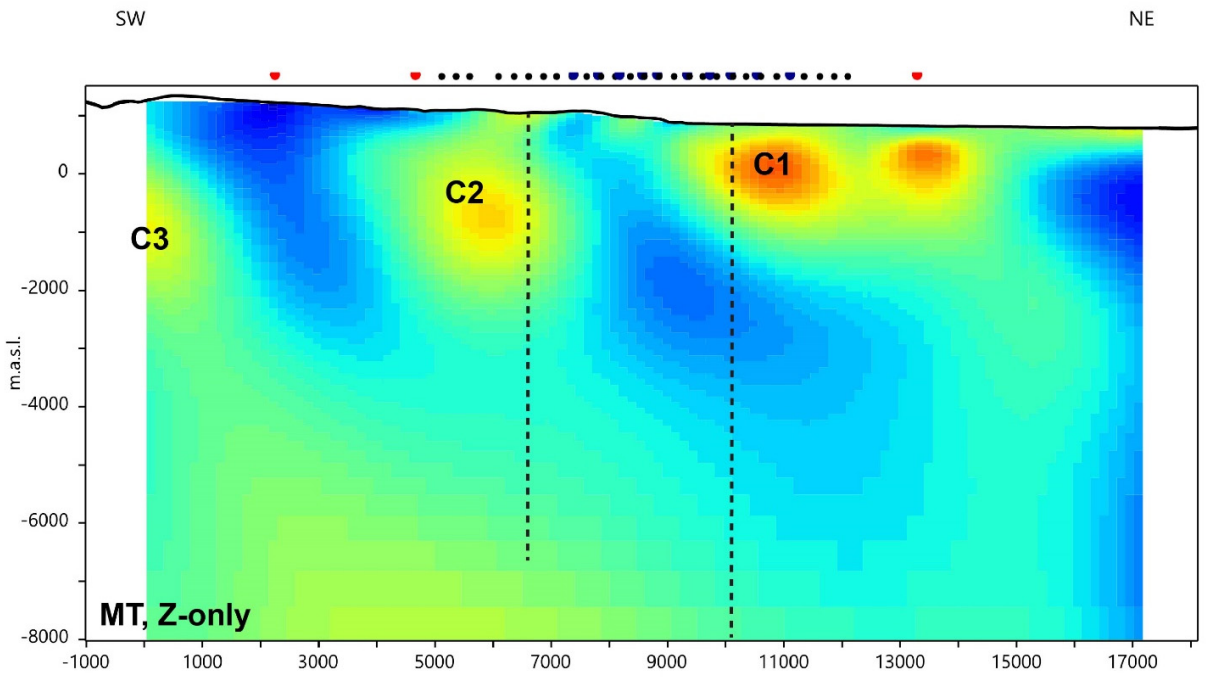
Table S1. Model parameter testing. Bold values were used for the preferred model (Figures 5, 6).


SW
NE
C2
C1
0
-2000
-4000
-6000
-8000
m.a.s.l.
ELF-EM, Tz-only
-1000
1000
3000
5000
7000
9000
11000
13000
15000
17000

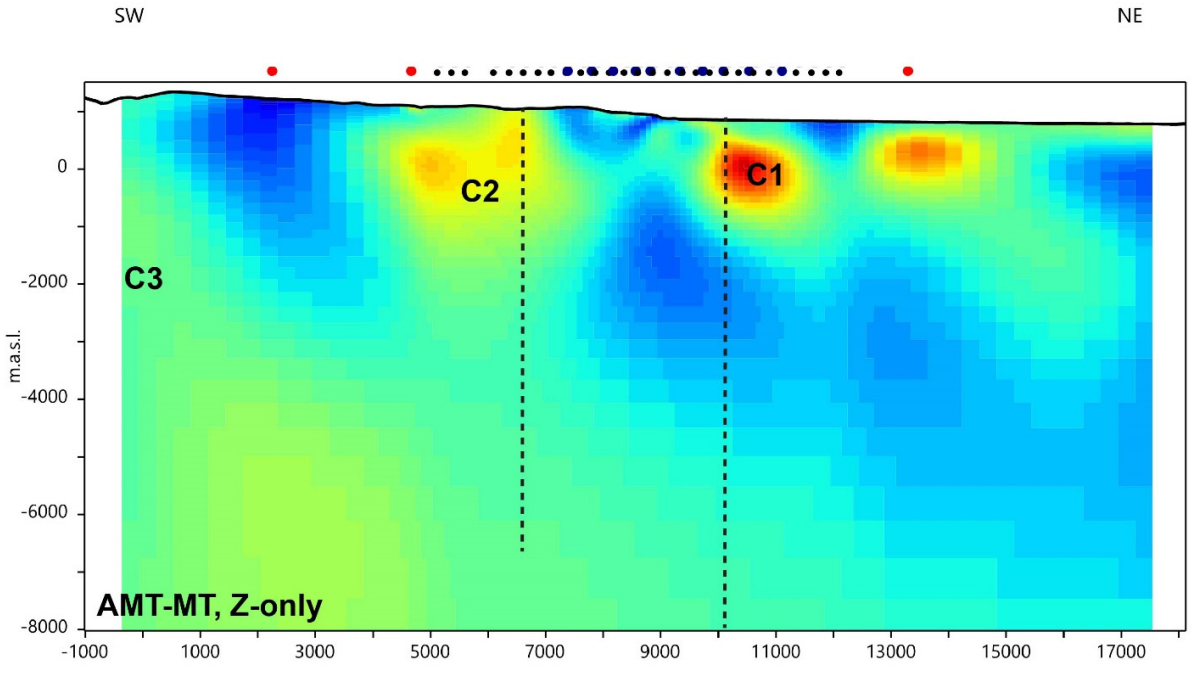
(a)


SW
NE
C1
0
-2000
-4000
-6000
-8000
m.a.s.l.
AMT, Z-only
-1000
1000
3000
5000
7000
9000
11000
13000
15000
17000

(b)


SW
NE
C1
C2
C3
MT, Z-only
m.a.s.l.
0
-2000
-4000
-6000
-8000
-1000
1000
3000
5000
7000
9000
11000
13000
15000
17000

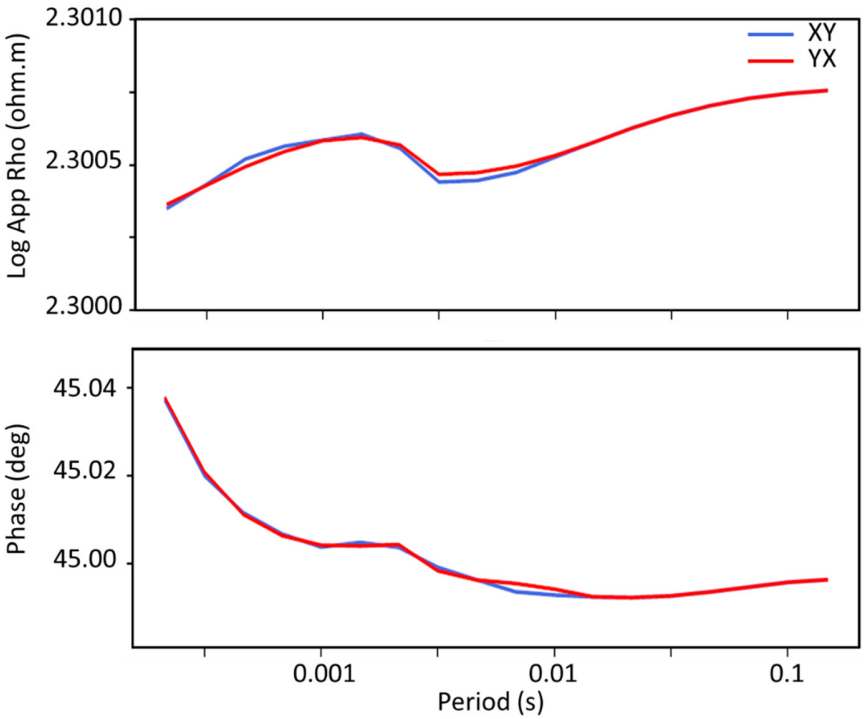
(c)


SW
NE
C1
C2
C3
AMT-MT, Z-only
m.a.s.l.
0
-2000
-4000
-6000
-8000
-1000
1000
3000
5000
7000
9000
11000
13000
15000
17000

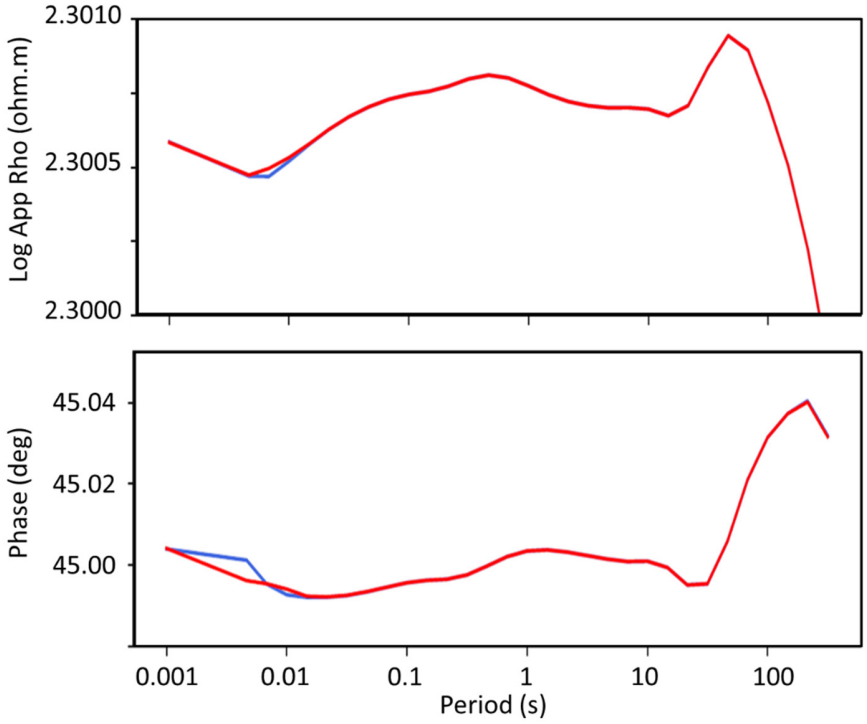
(d)

Figure S2: Cross-section over B-B’ (Figure 6b) using various passive EM datasets. a) ELF-EM; b) AMT; c) MT; and d) AMT-MT inversion with no vertical magnetic field (Tz) data.

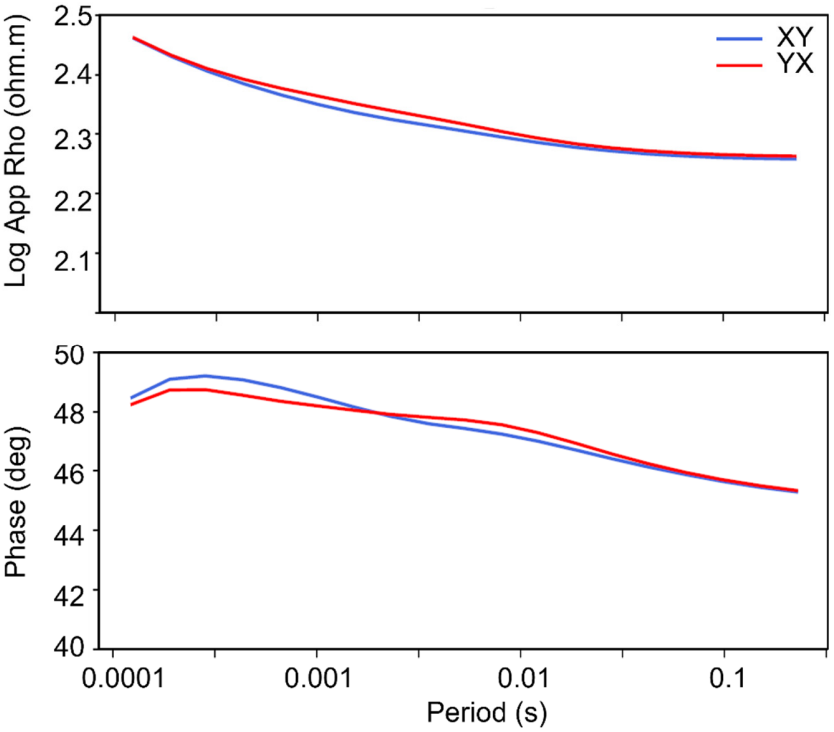
a) AMT69



b) MT11



c) AMT69



d) MT11

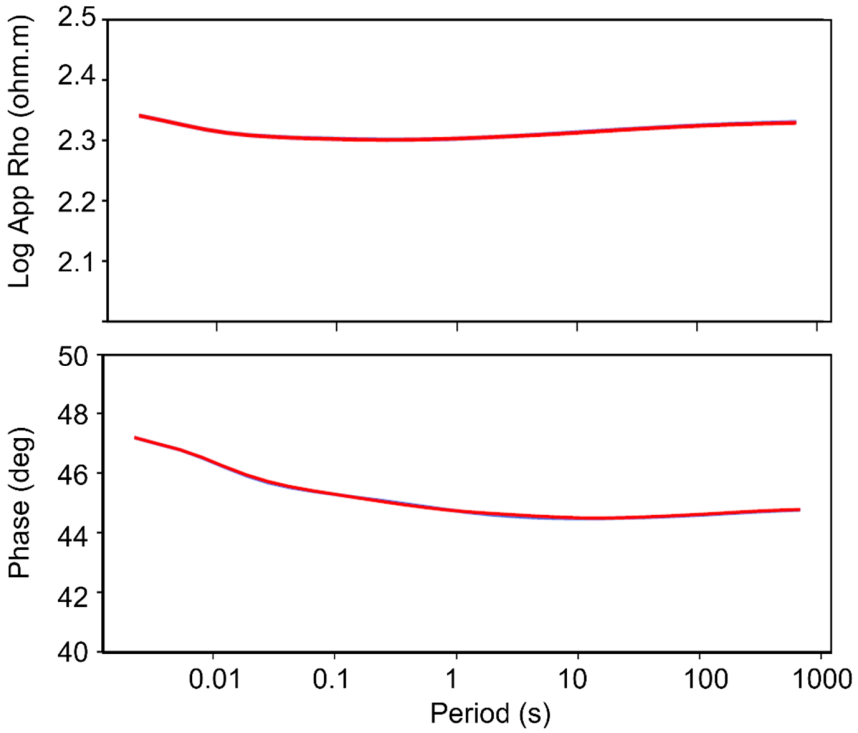
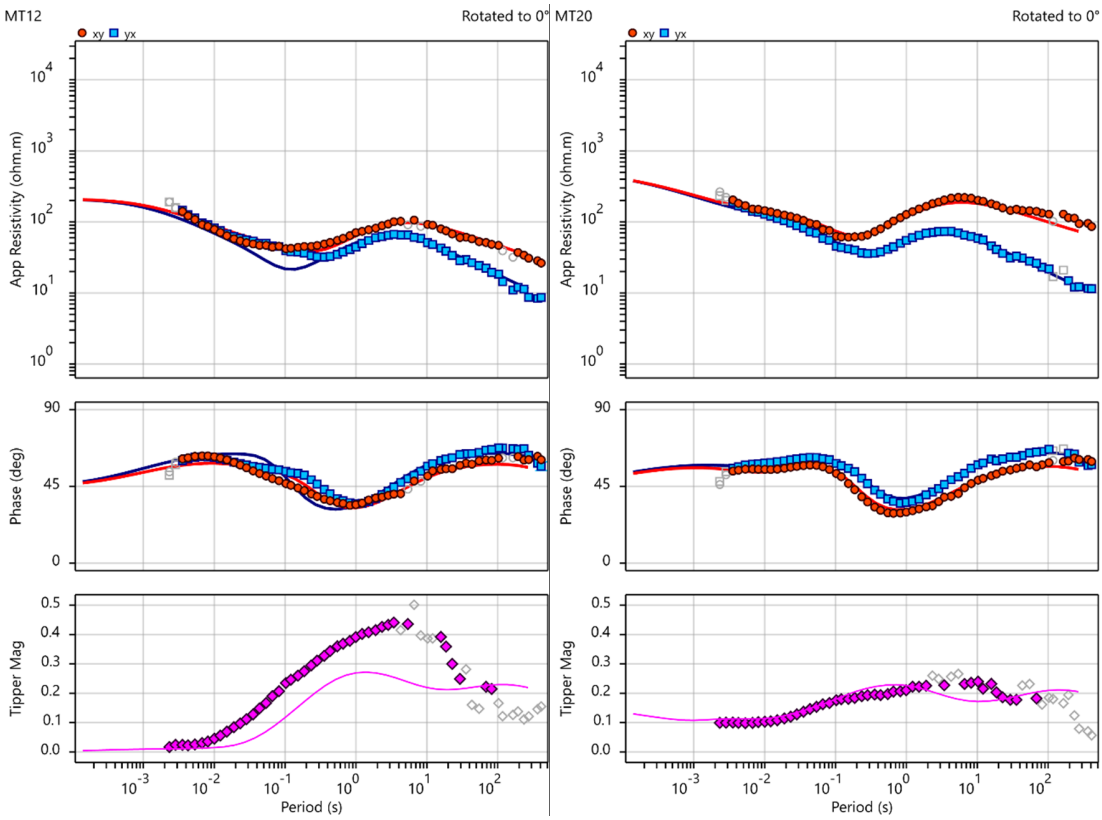
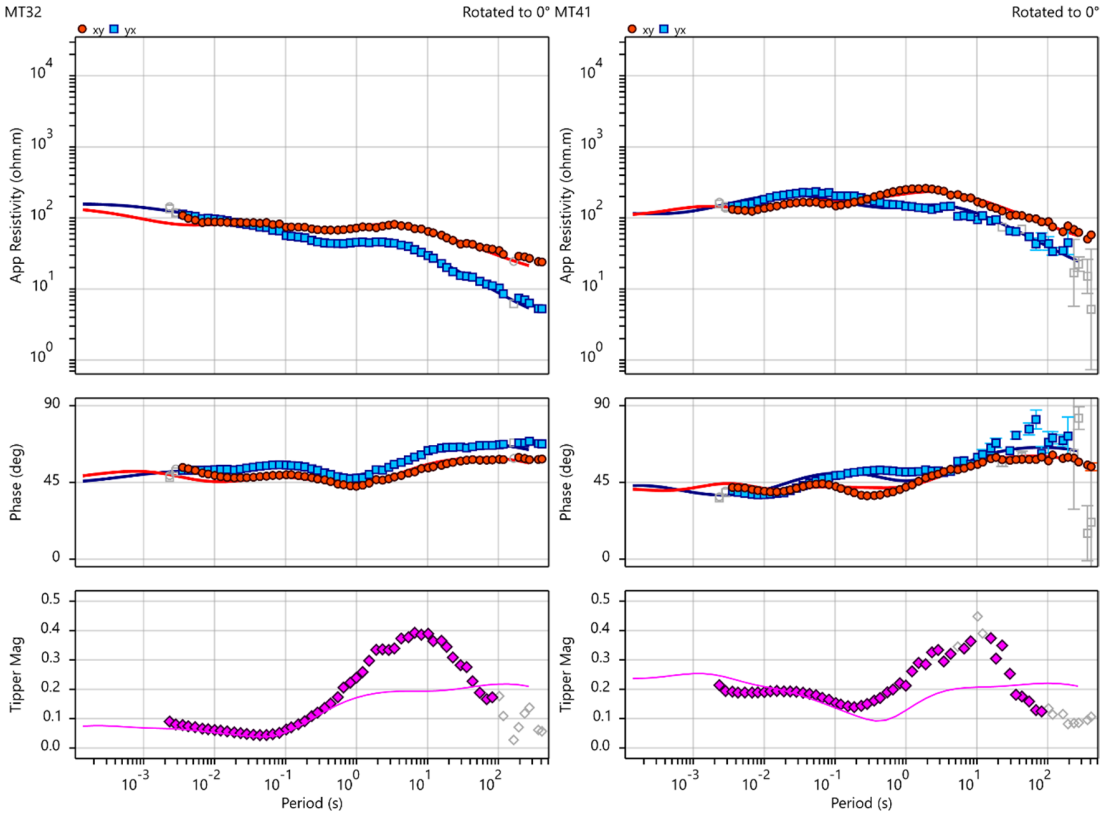
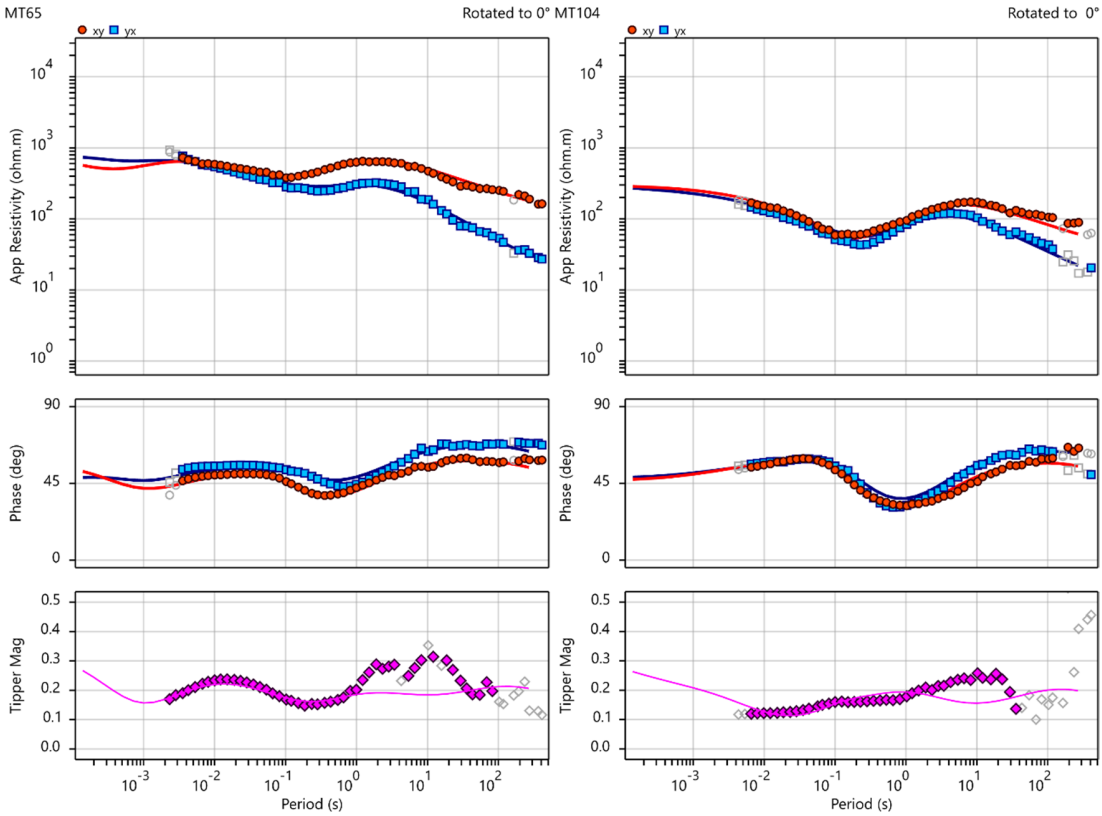
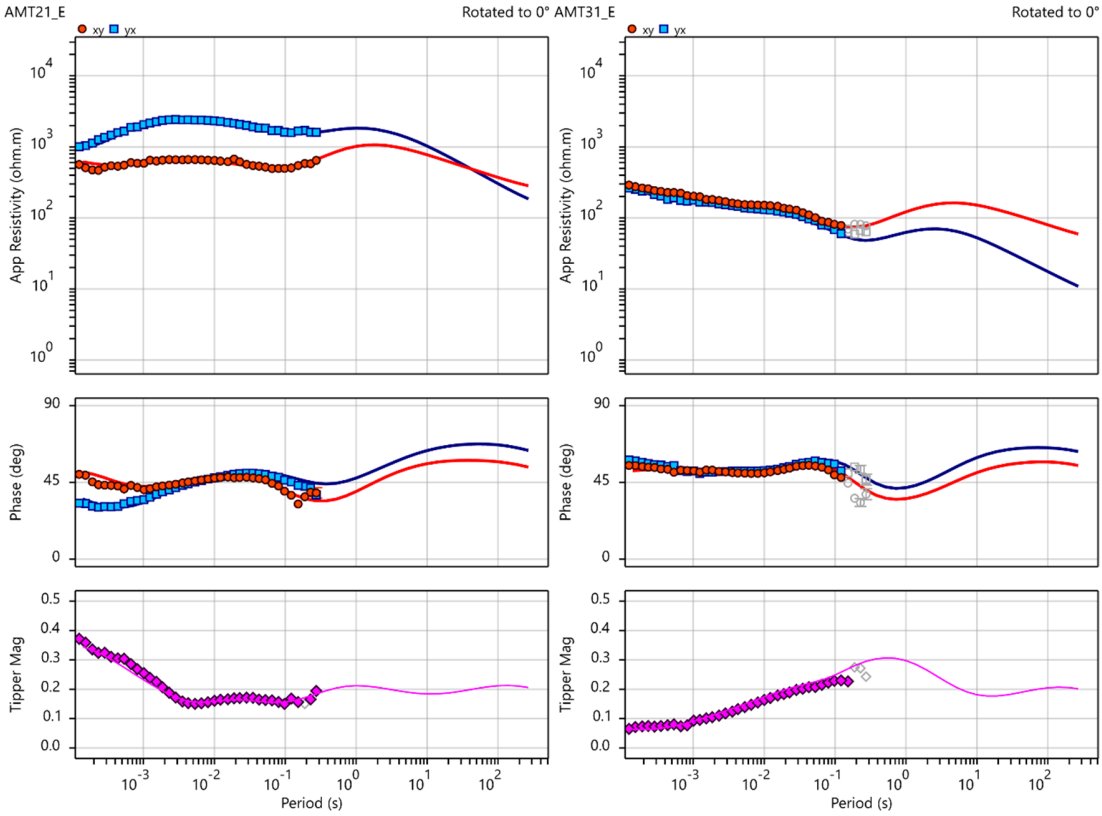


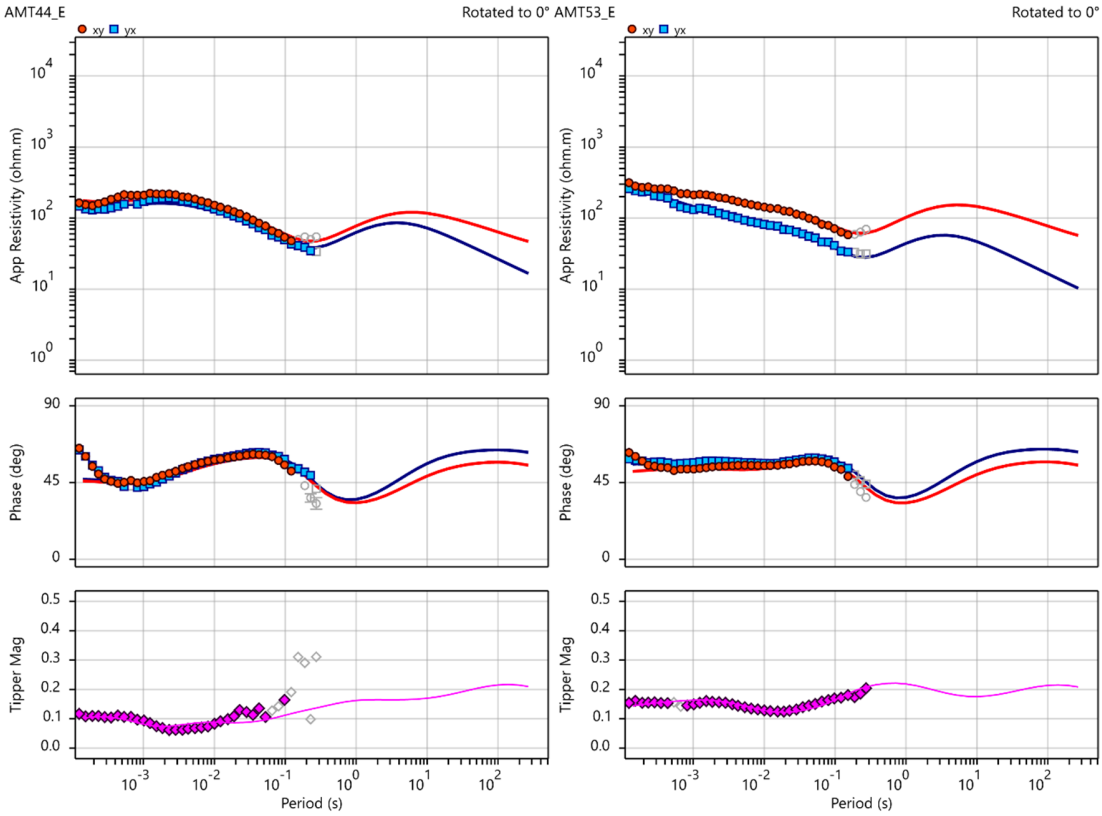
Figure S3: Forward tests of 200 Ωm half-space models including: a) and b) no topography versus c) and d) topography in one AMT and one MT station (from Table S1). The estimated XY and YX components are represented by red and blue lines, respectively.


MT12
Rotated to 0°
xy
yx
App Resistivity (ohm.m)
Phase (deg)
Tipper Mag
Period (s)
MT20
Rotated to 0°
xy
yx
App Resistivity (ohm.m)
Phase (deg)
Tipper Mag
Period (s)


MT32
Rotated to 0° MT41
Rotated to 0°
xy
yx
App Resistivity (ohm.m)
Phase (deg)
Tipper Mag
Period (s)


MT65
Rotated to 0° MT104
Rotated to 0°
xy
yx
App Resistivity (ohm.m)
Phase (deg)
Tipper Mag
Period (s)


AMT21_E
Rotated to 0° AMT31_E
Rotated to 0°
xy
yx
App Resistivity (ohm.m)
Phase (deg)
Tipper Mag
Period (s)


AMT44_E
Rotated to 0° AMT53_E
Rotated to 0°
xy
yx
App Resistivity (ohm.m)
Phase (deg)
Tipper Mag
Period (s)

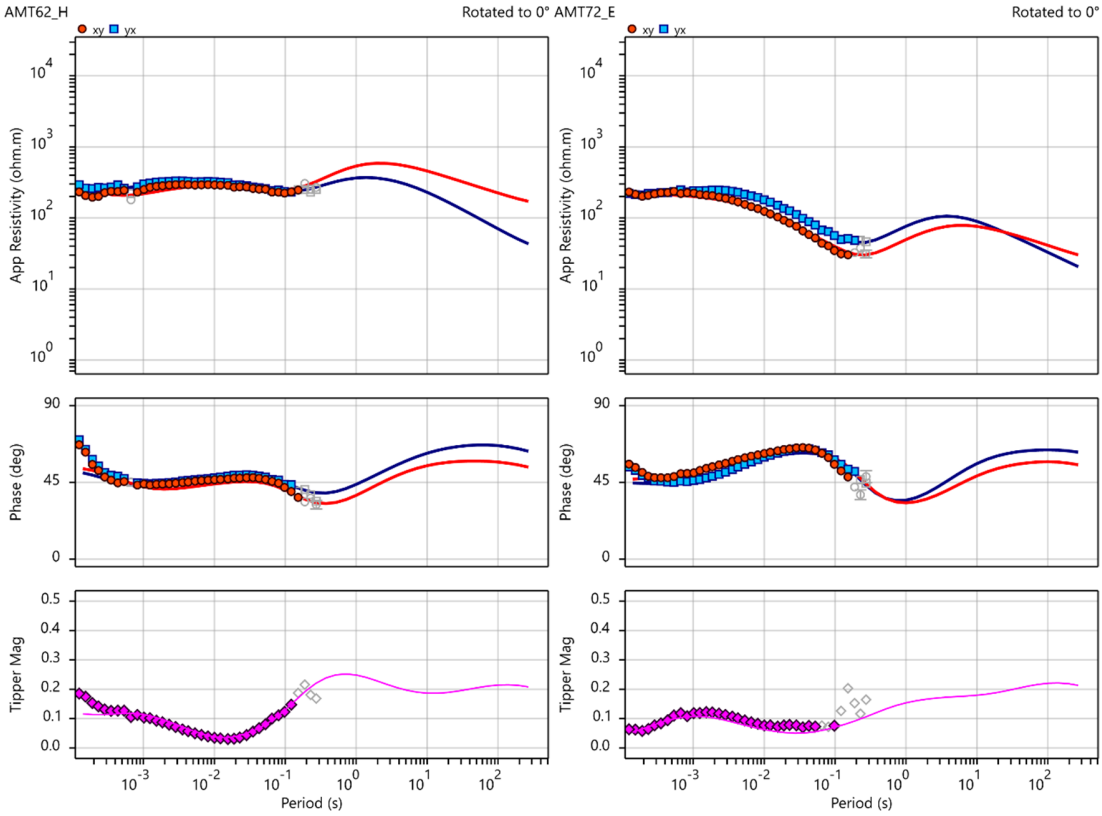
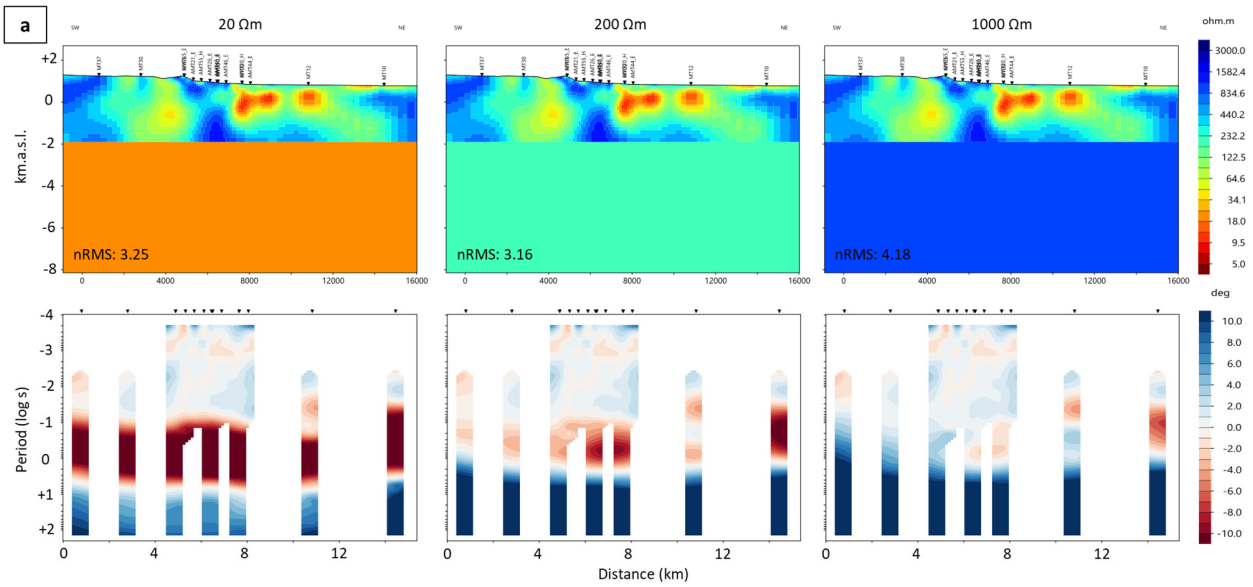


Figure S4: Measured (red circles (XY) and blue squares YX) and calculated (lines) apparent resistivity and phase curves for XY (red) and YX (blue) for 12 typical sites. Error bars plotted over the data as red or blue lines. Measured tipper plotted as pink squares and calculated tipper plotted as pink lines. Masked data are plotted in grey.

3. **Sensitivity Tests**

In order to test the influence of deeper features, we performed a set of forward tests on the preferred 3D resistivity model discussed in the paper (Figure S5). Compared with the RMS of the preferred model (1.04), the overall RMS was increased 117.3–301.9 % after running the depth assessment tests. The normalized determinant phase in each site's period range is shown in Figure S5. This figure provides a view of phase data fit across the entire profile and compares the phase responses of the test results and the raw data. Increasing the RMS and phase differences by perturbing the model

with different structures shows the sensitivity of data to solve for the depth of structures discussed in the paper. As expected, the model was less sensitive to the deepest features at 6 km; however they still resulted in an increase to the model nRMS with lower nRMS when higher conductivity features were added at 4 km and 6 km. As C3 was only present on the BBMT data due to the survey extents, additional testing was done on this feature by replacing it with the background resistivity (Figure S6a) which resulted in an increase in the station RMS and phase difference.



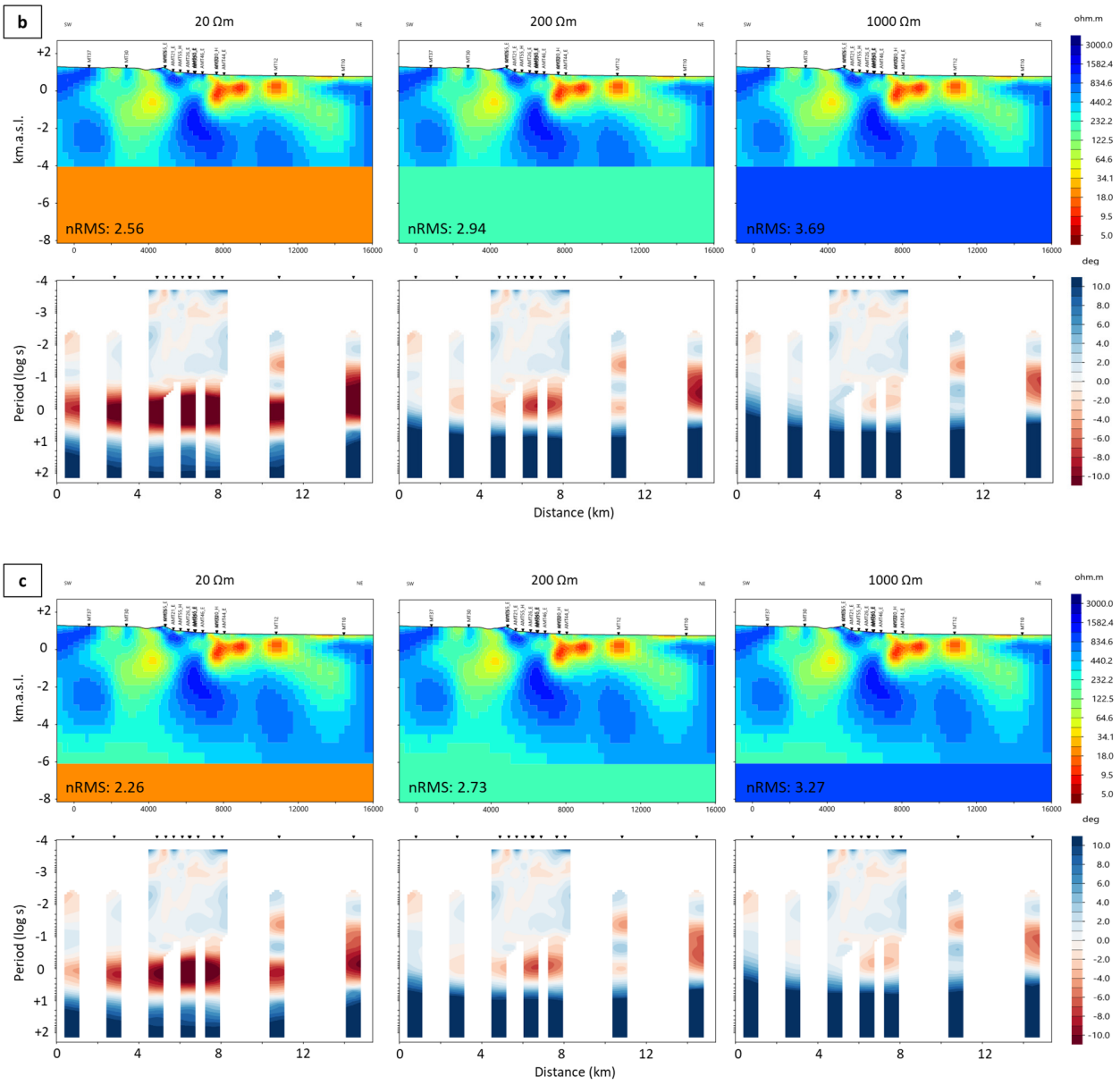
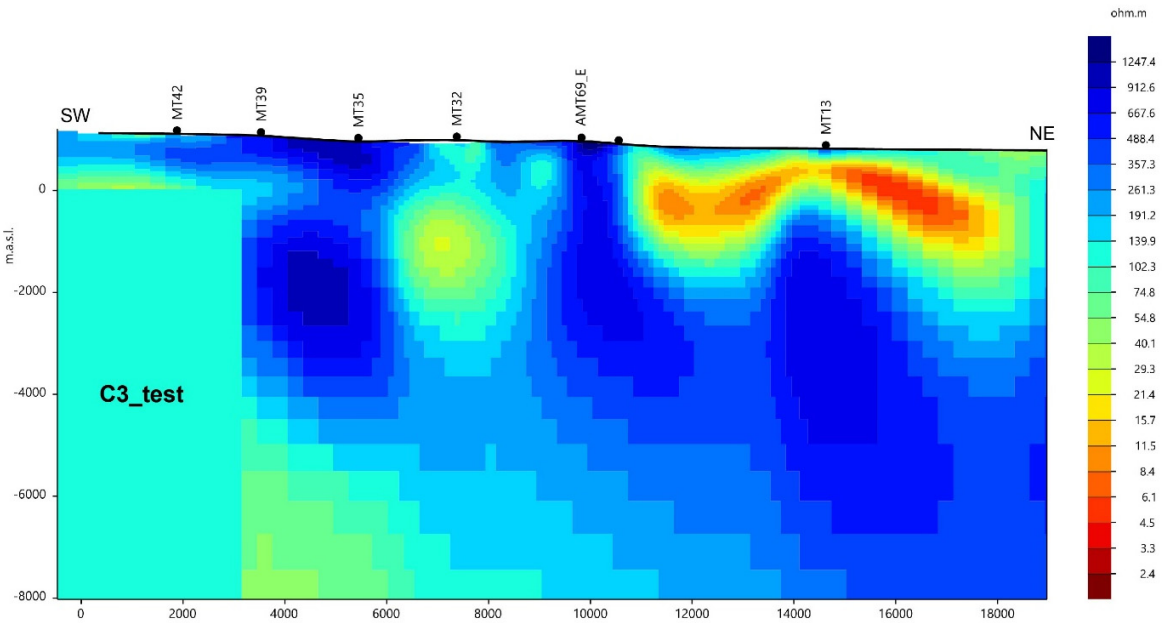


Figure S5: Normalized determinant phase pseudo-sections to assess the depth sensitivity of the model by introducing bodies with resistivities of 20 Ωm, 200 Ωm, and 1000 Ωm at: a) -2 km, b) -4 km, and c) -6 km depth. The nRMS of each test is shown at the bottom of each corresponding model.

(a)


SW
NE
MT42
MT39
MT35
MT32
AMT69_E
MT13
C3_test
m.a.s.l.
0
-2000
-4000
-6000
-8000
0
2000
4000
6000
8000
10000
12000
14000
16000
18000
ohm.m
1247.4
912.6
667.6
488.4
357.3
261.3
191.2
139.9
102.3
74.8
54.8
40.1
29.3
21.4
15.7
11.5
8.4
6.1
4.5
3.3
2.4

(b)

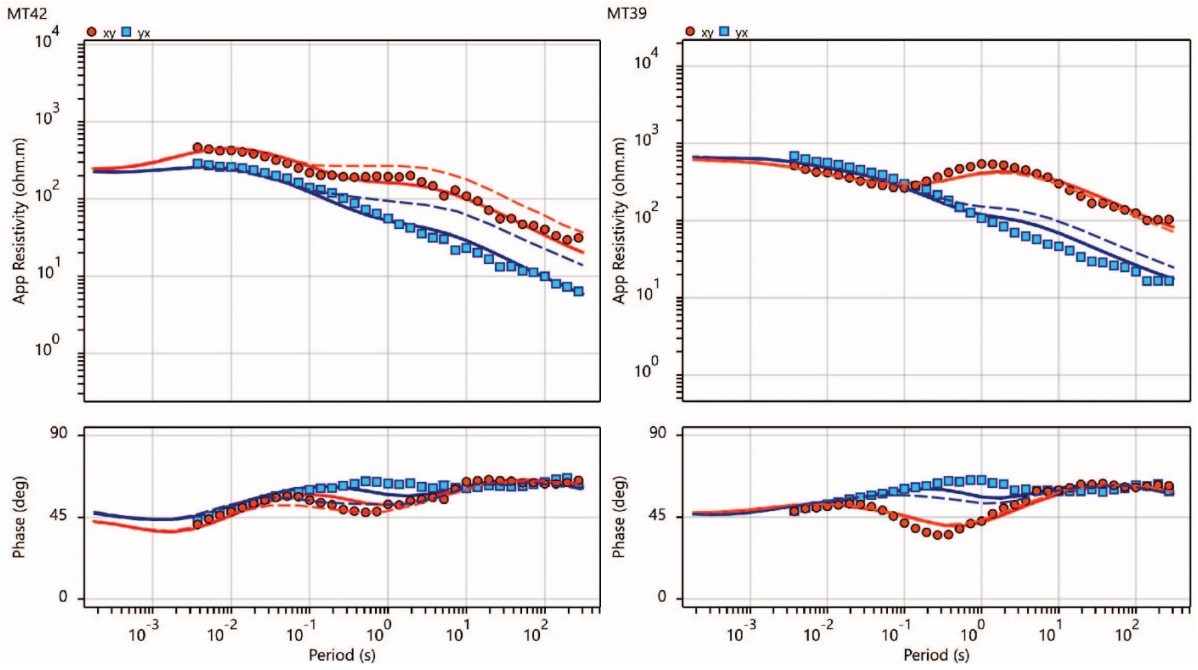

MT42
MT39
xy
yx
App Resistivity (ohm.m)
Phase (deg)
Period (s)

Figure S6: Sensitivity test on C3 by replacement with 200 Ωm background resistivity. a) SW-NE cross-section showing the C3 feature test. b) Apparent resistivity and phase as functions of period for closest sites to the C3 test. Solid and dashed lines show the results of forward response of preferred inversion and forward response with C3 replaced with a 200 Ωm body.

4. Physical Rock Properties

Physical rock property measurements were acquired on samples collected as part of Witter (2020) using the methodology described in Enkin et al., (2012). While Table 1 shows the average (or logarithmic average) of the sampled geological units, Figure S7 shows the relationship between resistivity and porosity. The data roughly approximate Archie's Law (Archie, 1942) with electrical resistivity proportional to porosity. We can expect the fault damaged and clay altered rocks guide electrical current flow as is the case in the preferred model with C1 and C2 localized over the major structures.

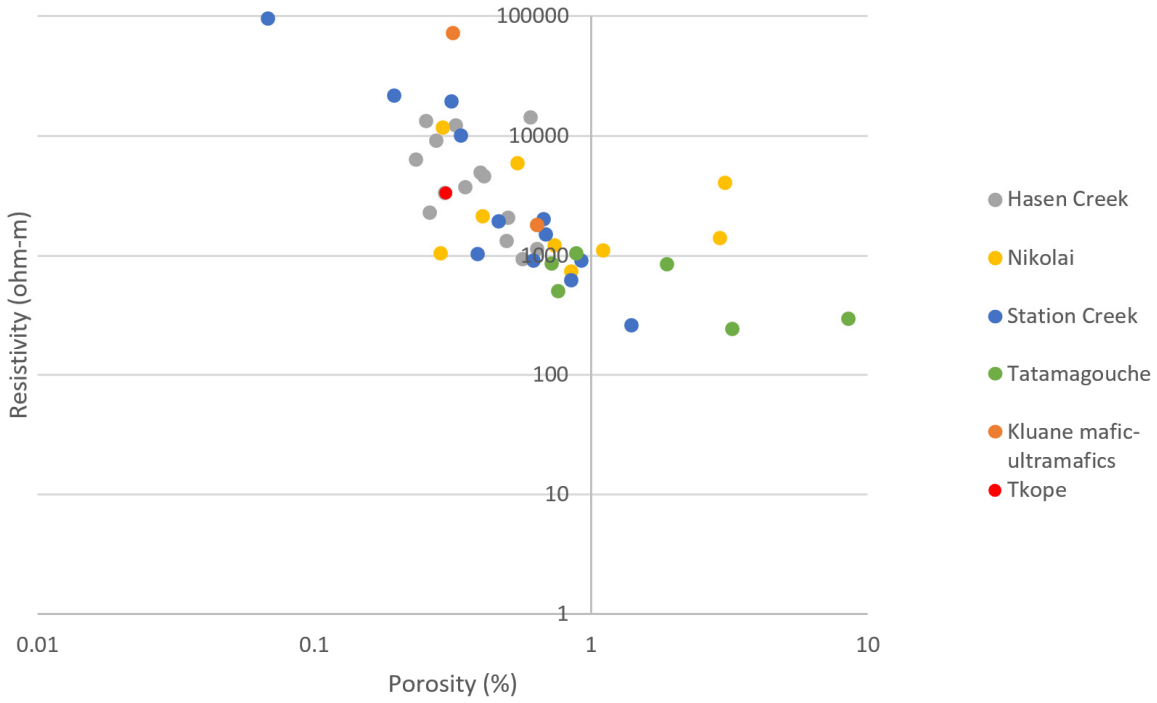


Figure S7: Resistivity versus porosity for samples from Table 1.

References

Archie, G.E., 1942. The electrical resistivity log as an aid in determining some reservoir characteristics. Transactions of the AIME, 146(01), 54-62.

Chave, A. D., Jones, A. G., 2012. The magnetotelluric method: Theory and practice. Cambridge University Press.

Enkin, R.J., Cowan, D., Tigner, J., Severide, A., Gilmour, D., Tkachyk, A., Kilduff, M., & Baker, J., 2012. Physical property measurements at the GSC Paleomagnetism and Petrophysics Laboratory, including electric impedance spectrum methodology and analysis. Geological Survey of Canada Open File, 7227, 57 p.

Quantec Geoscience, 2021. MT electrode comparison: porous pots vs. steel plates. Unpublished report.

Witter, J.B., 2020. Early-stage exploration for geothermal energy resources along the Denali fault near Duke River, Yukon. Yukon Geological Survey, Open File 2020-3, 70 p.